

# Liquid Chromatography–Mass Spectrometry–Based Qualitative Profiling of mRNA Therapeutic Reagents Using Stable Isotope-Labeled Standards Followed by the Automatic Quantitation Software Ariadne

Hiroshi Nakayama,<sup>#</sup> Yuko Nobe,<sup>#</sup> Masami Koike, and Masato Taoka\*



Cite This: *Anal. Chem.* 2023, 95, 1366–1375



Read Online

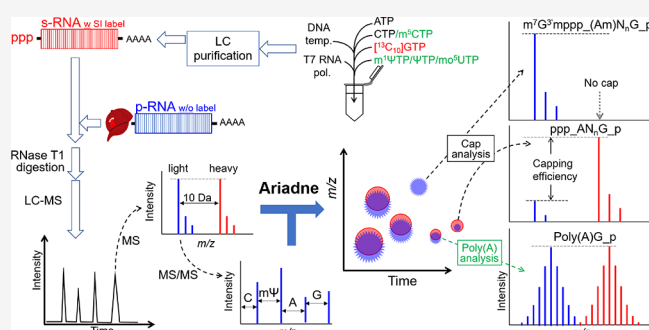
ACCESS |

Metrics & More

Article Recommendations

Supporting Information

**ABSTRACT:** mRNA-based medicines are a promising modality for preventing virus-caused illnesses, including COVID-19, and treating various types of cancer and genetic diseases. To develop such medicines, methods to characterize long mRNA molecules are needed for quality control and metabolic analysis. Here, we developed an analytical platform based on isotope-dilution liquid chromatography–mass spectrometry (LC–MS) that quantitatively characterizes long, modified mRNAs by comparing them to a stable isotope-labeled reference with an identical sequence to that of the target medicine. This platform also includes database searching using the mass spectra as a query, which allowed us to confirm the primary structures of 200 to 4300 nt mRNAs including chemical modifications, with sequence coverage at 100%, to detect/identify defects in the sequences, and to define the efficiencies of the 5'-capping and integrity of the polyadenylated tail. Our findings indicated that this platform should be valuable for quantitatively characterizing mRNA vaccines and other mRNA medicines.



## INTRODUCTION

Messenger RNA (mRNA)-based therapeutic reagents have great potential to revolutionize several areas of medicine. Because such mRNAs can be used to synthesize all kinds of proteins, this reagent is already being used as a vaccine to prevent serious illnesses from infection and is expected to be used in the future to treat various diseases including cancer and metabolic diseases.<sup>1–4</sup> In addition, this modality not only can be used to target a wide range of diseases but also includes a remarkable safety feature—namely, mRNA, which is not able to integrate into the host cell genome.<sup>3</sup> Such treatments are also advantageous in that mRNAs are relatively easy to manufacture and can readily be scaled up, thus reducing costs and the time to market.<sup>3,5</sup>

The following is an overview of certain mRNA medicines, using the Pfizer/BioNTech COVID-19 vaccine as an example.<sup>6,7</sup> This vaccine contains a long and single-stranded mRNA that encodes the spike glycoprotein of SARS-CoV2 including multiple antigens.<sup>8</sup> The mechanism of action of the vaccine is as follows: the mRNA corresponding to the antigen encoding gene is uptaken into a host cell; the cell expresses the protein; and the immune system recognizes the antigens included in the protein, causing an immune response. Each such mRNA strand has three common structural elements: a capping structure at the 5' end, a specific sequence for the

mRNA medicine, and a polyadenylated (poly(A)) tail at the 3' end.<sup>5</sup> The cap has a structure that initiates efficient translation and does not activate the innate immune system;<sup>9,10</sup> the specific sequence encodes the amino acid sequence with the relevant antigens and has a set of 5' non-coding, coding, and 3' non-coding sequences in which all uridines are replaced by N1-methylpseudouridine (m<sup>1</sup>Ψ), which attenuates the innate immune response against the RNA in vivo;<sup>6,11–13</sup> the poly(A) tail slows degradation of the mRNA by exonucleases, i.e., it prolongs the in vivo half-life by increasing the stability of the RNA, thereby enhancing RNA translation efficiency.<sup>14</sup>

It is necessary to develop an analytical platform that allows for the evaluation of individual mRNA medicines, as well as for the means to ensure their safety and effectiveness. MS-based methods for product characterization and quality control have recently begun to be reported; however, they are not compatible with quantitative assessment of various modified nucleosides,<sup>15,16</sup> cap structures, and poly(A) structures.<sup>17,18</sup>

Received: September 30, 2022

Accepted: December 14, 2022

Published: December 27, 2022



We here suggest an MS-based analytical platform using SILNAS<sup>19</sup> followed by data processing with the Ariadne software.<sup>20,21</sup> We describe the details of this experimental approach and show that the platform can be applied not only to validate modification of the specific sequence of the RNA reagent but also to analyze its capping structure and poly(A) tail.

## MATERIALS AND METHODS

**Reagents.** Standard laboratory chemicals were obtained from Wako Pure Chemical Industries. Sodium guanosine-<sup>13</sup>C<sub>10</sub> 5'-triphosphate (98 atom% <sup>13</sup>C) ([<sup>13</sup>C<sub>10</sub>]GTP) and RNase A were obtained from Sigma-Aldrich. 1-Methylpseudouridine-5'-triphosphate (m<sup>1</sup>ΨTP), 5-methylcytidine-5'-triphosphate (m<sup>5</sup>CTP), 5-methoxyuridine-5'-triphosphate (mo<sup>5</sup>UTP), pseudouridine-5'-triphosphate (ΨTP), and cap 1 analog (m<sup>7</sup>G<sup>3'</sup>mppp\_(Am)G\_OH, CleanCap Reagent AG(3'OMe)) were obtained from TriLink. RNase T1 was purchased from Worthington and further purified by reversed-phase liquid chromatography (RPLC) before use. Triethylammonium acetate (TEAA) solution (2 M, pH 7) was purchased from Glen Research.

**PCR Procedure.** Oligos were obtained from Fasmac Co., Ltd. The sequences are included in Table S1. PCR was carried out in a thermal cycler (MJ Mini, Bio-Rad) for 30 cycles (each consisting of 10 s at 98 °C, 15 s at 60 °C, and 20 s at 68 °C). Primers (10 pmol of each) and 2.5 U of PrimeSTAR GXL DNA Polymerase (Takara Bio) were used for each reaction in a volume of 50 μL, using the reaction buffer recommended by the polymerase supplier.

**DNA Templates for In Vitro Transcription of RNA Reagents.** The template DNA for the BNT162b2-mimicking RNA (mimBNT162b2) was constructed based on the report by Pfizer/BioNTech<sup>6</sup> with the addition of the T7 promoter (Table S1). The poly(A) region was segmented to reduce length variation due to recombination.<sup>22</sup> The DNA, which was chemically synthesized and inserted into the plasmid pANT, was obtained from Biologica Co., Ltd., and sequenced by standard procedures. The sequence was confirmed except for the poly(A) segments. Both of the segments contained heterogeneities of several residues in length. The reason for the heterogeneity is that cloning the poly(A)-containing DNA into a plasmid makes the homopolymer A–T base pairs in the vector unstable and prone to shortening during replication in bacteria.<sup>23,24</sup>

DNA templates for in vitro transcription of RNA1, RNA1mut, RNA1trn, and RNA1ext were produced by the same PCR procedure using t-VcovSmp11F/t-VcovSmp11R, t-VcovMut1F/t-VcovSmp11R, t-VcovSmp11F/t-VcovShortR, and t-VcovSmp11F/Cov19\_2R, respectively, as primer pairs (Table S1) and mimBNT162b2 DNA as the PCR template.

DNA templates corresponding to vaccine-like mRNAs for influenza A hemagglutinin, West Nile NS1, and Zika propep/M were made by overlap extension PCR.<sup>25</sup> In brief, to construct each PCR template, three cDNA pieces, corresponding to the 5' noncoding, 3' noncoding, and coding regions, were prepared by the PCR procedure. The 5' and 3' noncoding regions were amplified using Cov19Vac F/Cov19Vac5PR and Cov19Vac3PF/Cov19Vac3PR primer pairs, respectively, and mimBNT162b2 DNA as the template. These products were separated by agarose gel electrophoresis and were extracted with a QIAEX II Gel Extraction Kit (Qiagen). The coding regions were amplified using InfAVacF/

InfVacR, WNVacF/WNVacR, and ZiKAVacF/ZikaVacR as primer pairs and influenza A hemagglutinin (Addgene, Cat# 127810), West Nile NS1 (Addgene, Cat# 52882), and Zika propep/M (Addgene, Cat# 79631) DNAs as the templates, respectively. After amplification, the PCR reactions from the 5' and 3' noncoding and the coding regions were mixed at a molar ratio of 1000:1000:1. Using the resulting mixture as a template and Cov19Vac F/Cov19Vac3PR as the primer pair, overlap extension PCR was performed to produce an in vitro transcription template (Table S2). The resulting PCR products were all directly sequenced, which confirmed the presence of the expected sequence, although the products showed heterogeneity with respect to the length of their poly(A) tails. This heterogeneity is known to occur with in vitro experiments such as PCR.<sup>26,27</sup> These PCR products were cloned into a vector (T-Vector pMD19, Takara Bio). The cloned DNA sequences were confirmed and contained heterogeneities of several residues in the length of the poly(A) tail again, although it was more homogenous than before the cloning. The cloned DNAs were also used as templates for in vitro transcription.

**Preparation of RNAs.** Each RNA was generated from its corresponding DNA template digested with HindIII using an in vitro transcription kit (MEGAscript T7 Kit, Thermo Fisher Scientific) in the presence of m<sup>1</sup>ΨTP, ΨTP, or mo<sup>5</sup>UTP instead of uridine-5'-triphosphate (UTP) and/or in the presence of m<sup>5</sup>CTP instead of cytidine-5'-triphosphate. The 5'-capping structure was synthesized co-transcriptionally using a cap 1 analog. The RNA was purified from the reaction (~15 μg) by RPLC on a PLRP-S 300 Å column (2.1 × 150 mm, 3 μm; Agilent Technologies) or a 4000 Å column (4.6 × 150 mm, 8 μm; Agilent Technologies)<sup>28</sup> and stored at –80 °C.

**Direct Nanoflow LC–MS and LC–MS/MS Analysis of RNA Fragments.** RNA was digested with RNase T1 or A (~4 ng/μL) in 100 mM TEAA solution (pH 7.0) at 37 °C for 60 min. The nucleolytic RNA fragments were injected into a reversed-phase column (150 μm i.d. × 240 mm) that had been equilibrated with solvent A (10 mM TEAA, pH 7, in 9:1 [v/v] water/methanol). The column was slurry packed in-house with Develosil C30-UG (3 μm particle size; Nomura Chemical Co., Ltd.).<sup>27</sup> The RNA fragments were eluted with a 60 or 120 min 0–24.5% linear gradient of solvent B (6:4 [v/v] 10 mM TEAA, pH 7/acetone) at a flow rate of 200 nL/min, as described.<sup>29,30</sup> For the detection of RNA fragments of >30 residues, a 60 mm column was equilibrated with solvent A and eluted with a 30 min 0–40% linear gradient of solvent B at a flow rate of 100 nL/min. The LC eluate was sprayed online at –1.3 kV with the aid of a spray-assisting device<sup>30</sup> to introduce the sample into a Q Exactive mass spectrometer (Thermo Fisher Scientific) in negative ion mode. The spectrometer was operated in a data-dependent mode to automatically switch between MS and MS/MS acquisition. A high-energy collisional dissociation cell was used to read RNA sequences with normalized collision energy of 20%. Full-scan mass spectra (from *m/z* 480 to 1980) were acquired at a mass resolution of 35,000 or 140,000. The five most intense mass peaks, each with an intensity of >50,000 counts/s (maximum injection time, 60 ms), were isolated within a 3 *m/z* window for fragmentation. A mass resolution of 17,500 at *m/z* 200 for MS/MS was set to derive the nucleotide sequence from the fragment ions of the RNA digests. To retain mass resolution and to increase spectral quality, three MS/MS micro-scans

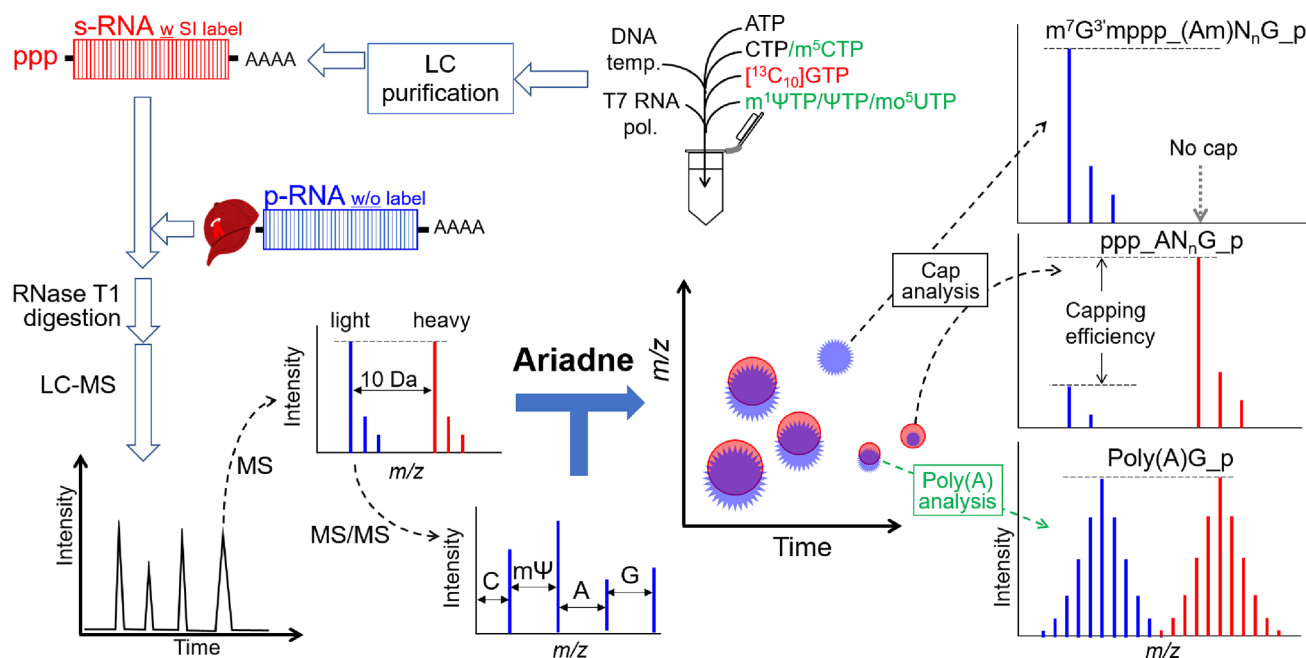


**Figure 1.** Strategy for quality control of mRNA medicines. Synthesis of standard RNA (s-RNA) and analysis of the internal sequence of the test RNA (i.e., pharmaceutical RNA or p-RNA) used as an mRNA medicine and quantitative analysis of the cap and poly(A) structure are shown. A detailed explanation is given in the text.  $m^{13}C_{10}$ , 1-methylpseudouridine;  $m^5C$ , 5-methylcytidine;  $m^5U$ , 5-methoxyuridine;  $\Psi$ , pseudouridine; TP, 5'-triphosphate, SI, stable isotope.

were summed to obtain a final MS/MS spectrum. The starting mass value for acquisition of the MS/MS spectra was  $m/z$  100.

**Database Search and Interpretation of RNA MS/MS Spectra.** Ariadne was used for database searches, assignment of MS/MS spectra from RNA, and quantitation of RNA fragments.<sup>19–21</sup> The sequences resulting from the virtual cleavage of the mRNA medicines were used to make up an RNA database. The symbols for post-transcriptionally modified nucleosides used in the RNA sequences are referred to MODOMICS.<sup>31</sup> The 5' or 3' terminal phosphate (p), 2',3' cyclic phosphate (cp), or hydroxy (OH) groups in the sequences are separated by underscore letters (\_).<sup>20</sup> Default search parameters for Ariadne were used: maximum number of missed cleavages, one; variable modification parameters and unknown 58.005 Da modification (covalent adduction of  $C_2H_2O_2$ ), denoted as acoG, per any G residues; RNA mass tolerance,  $\pm 5$  ppm; and MS/MS tolerance,  $\pm 20$  ppm. For assignment of modified and stable isotope-labeled residues in RNAs, the variable modification parameter and isotope set were altered from default values to each modified residue and " $^{13}C_{10}_G$ ", respectively. The signature ion characteristic of  $m^7G^3'mp$ ,  $m^7G^3'mpp$ , and 2'-O-methylation at  $m/z$  390.07, 470.03, and 225.02, respectively, were used to assign the cap 1 analog identity. The extracted ion chromatograms were depicted using Xcalibur 3.0 software (Thermo Fisher Scientific) for the theoretical  $m/z$  ( $\pm 5$  ppm tolerance) of the RNase-digested fragments.

The term poly(A) integrity used in this study is defined as the ratio of MS signal intensities of p- and s-RNA fragments containing poly(A), which have a particular length that is equal to the most frequently found in the template DNA.

## RESULTS

**Principle of the Method and Workflow.** We have developed a platform to assess the quality of mRNA medicines

that have a natural isotopic distribution by comparing them to standard RNAs labeled with stable isotopes (Figure 1). Note that this method assumes that the standard RNA can be synthesized from the same template DNA as the mRNA medicine in an in vitro transcription system using T7 RNA polymerase, etc.<sup>6</sup> Standard RNAs are hereafter denoted with the prefix "s-". In contrast, test RNAs in the form used as pharmaceuticals are denoted with the prefix "p-". This method consists of two steps: preparation of s-RNA and assessment of target p-RNA by comparison with the s-RNA, as described below.









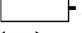
**Preparation of an s-RNA.** During the synthesis, s-RNA is transcribed in vitro with guanosine- $^{13}C_{10}$  and no capping analog (Figure 1). The 5'-capping structure of the s-RNA is left as triphosphate, the importance of which is explained in the next step. Because the s-RNA is a reference, it should be sufficiently purified, and its sequence should be confirmed. Therefore, it is appropriate for the s-RNA to be purified by RPLC, for example, before being cleaved by RNase T1 or A. Each resulting RNA fragment is then thoroughly characterized by LC-MS/MS to confirm the sequence of the original s-RNA.

**Assessment of Target mRNA Medicines.** p-RNA is prepared by the standard procedure for a target mRNA medicine. Each p-RNA contains a capping structure and guanosine in a natural isotope distribution, in contrast to the corresponding s-RNA. Then, the p-RNA is mixed with the s-RNA at a 1:1 ratio and cleaved with RNase T1, which hydrolyzes the 3' end of guanosine in RNA (Figure 1). The resulting RNA fragments include a pair of guanosine- $^{13}C_{10}$ -labeled and -unlabeled forms with the same sequence. Therefore, when this mixture is analyzed by LC-MS, the LC peak of the fragments of the s- and p-RNAs overlaps, and a pair of MS signals with a difference of 10 Da should be detected in the MS spectrum of each LC peak. By examining

the ratio of the intensities of the signal pairs, the specific sequence for p- or s-RNA can be evaluated. With this method, all RNA fragments without sequence defects exhibit single chromatographic peaks containing the unlabeled “light” and labeled “heavy” RNA fragments with identical signal intensities, whereas a light fragment carrying defects, such as a deletion, insertion, or replacement, does not appear at all or appears in a separate peak with a different chromatographic retention time relative to the corresponding heavy fragment derived from the s-RNA. Thus, even defects found in long RNAs can be accounted for by searching for the light fragments, and the type and position of the defects can be identified from their MS and MS/MS spectra. The method also provides quantitative information about defects; namely, we can estimate the amount of defective molecules in the p-RNA based on their signal intensities. Note that when the reproducibility of retention time during LC and the accuracy from MS analysis are sufficient, MS/MS is not required in the second step in most cases, although the structure of any impurities will not be determined.

The capping efficiency of the 5′ end can be examined by comparing the 5′-triphosphorylated fragments between the s- and p-RNAs (Figure 1). The percentage of the full-length 3′-poly(A) tail-containing fragment can also be determined by comparing the tail fragments between the s- and p-RNAs. However, in this case, the RNA needs to be engineered in a format where the guanosine that marks RNase T1 hydrolysis is on the 3′ side relative to the poly(A) sequence.

**Proof-of-Principle Experiment for mRNA-Based Reagents. Purification and Characterization of s-RNA1.** To demonstrate the concept, we examined RNA1, which mimics the 3′ region of BNT162b2<sup>6</sup> with a length of ~210 bases. The sequence contains 5′ and 3′ noncoding regions, the latter of which includes an A<sub>30</sub> poly(A) tail, and a coding region (Figure 2 and Table S2). RNA1 was synthesized with T7 RNA polymerase in the presence of RNA1-encoding DNA with the promoter sequence added to the 5′ region of the template (Table S1). For the synthesis of s-RNA1, m<sup>1</sup>ΨTP and [<sup>13</sup>C<sub>10</sub>]GTP were used instead of UTP and GTP, respectively,

RNA	Structure	Cap	[ <sup>13</sup> C <sub>10</sub> ]G	modified nucleosides
s-RNA1		—	+	m <sup>1</sup> Ψ
p-RNA1		+	—	m <sup>1</sup> Ψ
p-RNA1mut		+	—	m <sup>1</sup> Ψ
p-RNA1trn		+	—	m <sup>1</sup> Ψ
p-RNA1ext		+	—	m <sup>1</sup> Ψ
s-RNA1mod1		—	+	Ψ/m <sup>5</sup> C
p-RNA1mod1		+	—	Ψ/m <sup>5</sup> C
s-RNA1mod2		—	+	mo <sup>5</sup> U/m <sup>5</sup> C
p-RNA1mod2		+	—	mo <sup>5</sup> U/m <sup>5</sup> C

100 bases

**Figure 2.** Schematic structure of RNA used for the method validation and characteristics. The white and black rectangles represent the protein-coding region and mutation site, respectively. m<sup>1</sup>Ψ and Ψ are modified nucleosides used instead of uridine, and mo<sup>5</sup>U and m<sup>5</sup>C are modified nucleosides used instead of cytosine. The cap used here was m<sup>7</sup>G<sup>3</sup>mppp\_(Am)G\_OH.

to incorporate m<sup>1</sup>Ψ and [<sup>13</sup>C<sub>10</sub>]G into the RNA instead of uridine and guanosine, respectively (Figure 2). s-RNA1 was purified by RPLC, which resulted in a purity of >95% after shorter products were removed (Figure S1A) and was cleaved by RNase T1 or A, and each resulting digest was subjected to LC–MS analysis. The MS and MS/MS spectra were easily assigned by Ariadne to the s-RNA1 sequence, with the exception of the poly(A) cluster region, resulting in 100% sequence (Figure S1B) and quantitative coverage of the internal sequence. The poly(A) cluster region was also verified to be covered by manual inspection of the data (Figure S1C). In addition, we identified several fragments that cannot be explained by the template sequence, including OH\_CC\_OH and OH\_CG\_p. Meanwhile, almost all major MS/MS spectra were consistent with the RNA1 sequence (data not shown), showing that the purification eliminated major contaminants. These results indicated that this s-RNA1 preparation was of sufficient purity and was consistent with the template DNA sequence.

**Analysis of the Integrity of an mRNA Medicine Sequence.** We synthesized p-RNA1 (Figure 2 and Table S2) and purified it by RPLC. p-RNA1 was produced from the same template as s-RNA1 with the cap 1 analog m<sup>7</sup>G<sup>3</sup>mppp\_(Am)G\_OH and GTP that contained atoms with a natural isotope distribution. p-RNA1 was mixed 1:1 with s-RNA1, the mixture was cleaved with RNase T1, and the resulting RNA fragments were analyzed by LC–MS. Pairs of LC–MS peaks corresponding to s- and p-RNA1 fragments exhibited the expected mass difference of 10 Da (Figure S2). To provide an overview of this analysis, we present the data as a bubble chart that indicates the retention time during LC and the *m/z* and signal intensity from MS of the RNA fragments (Figure 3 and Table S3). All bubbles derived from RNA fragments of s- and p-

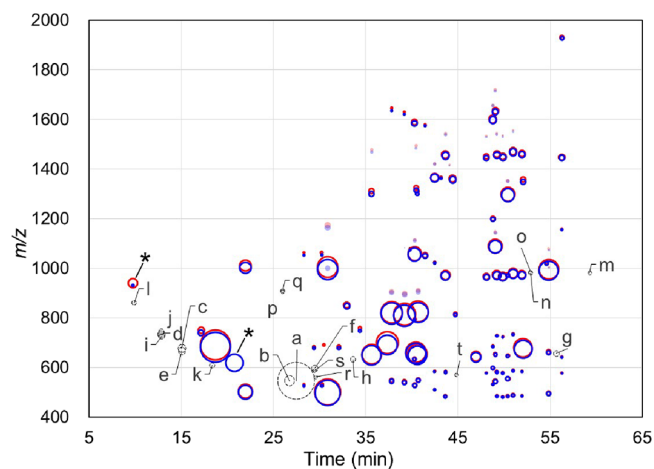


**Figure 3.** Bubble chart displaying the analysis of s- and p-RNA1. Retention time during LC (horizontal axis), the *m/z* (vertical axis), and the signal intensity (bubble size) value of each RNA fragment obtained from Ariadne were plotted on a bubble chart. Classification of RNA bubbles, red—s-RNA1, blue—p-RNA1, dashed gray—not predicted from template sequence. \*, S′-end fragment with or without cap 1. Bubbles indicating adduct ions are filled with their respective colors. Only ions with MS/MS signals characteristic of ribose (*m/z* 211.00) are displayed to exclude signals not related to RNA. Among the RNA fragments not expected from the template sequence, the top 20 with respect to signal intensity are shown in the figure along with their unique alphabetical symbols. The assignment of each bubble (i.e., its short label) is presented in Table S3.

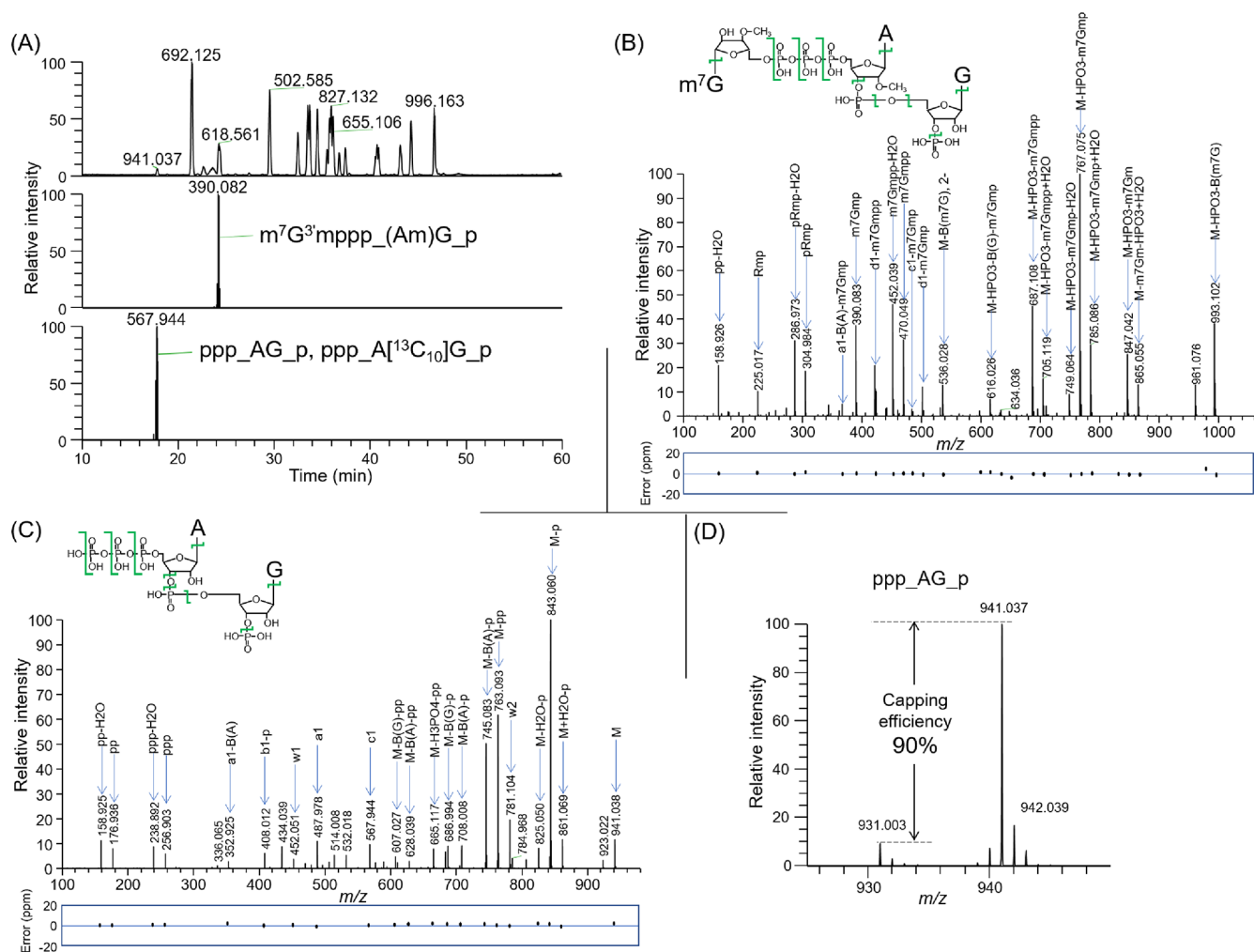


**Figure 4.** Selective detection and quantitation of cap 1 in p-RNA1. (A) Mass chromatograms of the RNA fragment containing the cap-related structure. The 1:1 mixture of s- and p-RNA1 (each 100 fmol) was digested with RNase T1, and the resulting fragments were subjected to LC–MS and –MS/MS. The base peak chromatogram is shown at the top. The signals extracted in the MS/MS step were at  $m/z$  390.082 and 567.944 for  $m^7G^{3'}mp$  and  $pppA$ , respectively (middle and bottom). The sequences assigned by Ariadne are shown next to their signals. Note that both  $ppp\_AG\_p$  and  $ppp\_A^{[13C_{10}]G\_p}$  fragments produce  $pppA$ ; thus, there are two assignments to one peak. (B, C) MS/MS spectrum of (B)  $m^7G^{3'}mppp\_p(Am)G\_p$  in p-RNA1 and (C)  $ppp\_A^{[13C_{10}]G\_p}$  in s-RNA1. The  $m/z$  value and sequence in the spectrum identify the major a, b, c, and d and w, x, y, and z ions, respectively.<sup>32</sup> The cleavage positions of the assigned ions are mapped on the RNA structure of each panel (green). Errors determined by Ariadne in the MS/MS signals are plotted under each spectrum. m,  $CH_2$ ; p,  $HPO_3$ ; pp,  $H_4P_2O_7$ ; ppp,  $H_5P_3O_{10}$ ; R,  $C_5H_8O_4$ ;  $m^7G$ , 7-methyl guanosine; –, neutral loss;  $-B(N)$ , neutral loss of nucleobase. (D) SILNAS-based cap analysis. In an LC–MS analysis, the light fragment  $ppp\_AG\_p$  and the corresponding heavy fragment  $ppp\_A^{[13C_{10}]G\_p}$  were detected from the p- and s-RNA1 mixture.

RNA1 were detected as doublets of the same size in the figure except for the 5'-end, poly(A) region, and some G-free fragments. This result indicated that the fragment derived from p-RNA1 is the same as that from s-RNA1 with respect to quality and quantity; namely, p-RNA1 had the same sequence of the same length as did s-RNA1, except around the 5' cap and 3' poly(A) sequences.

**Measurement of Capping Efficiency.** Next, we analyzed the 5'-end fragments of s- and p-RNA1. In Figure 3, the 5' end fragments are shown as a bubble doublet with two bubbles of different sizes and as a single bubble (indicated by an asterisk). The double bubbles and single bubbles were derived from  $ppp\_AG\_p$  of the s- and p-RNA1 without the cap 1 analog and  $m^7G^{3'}mppp\_p(Am)G\_p$  of p-RNA1 with the cap 1 analog, respectively (Figure 4A). The structure of the fragments with or without the cap 1 analog was confirmed by MS/MS ion analysis using Ariadne (Figure 4B,C). By comparing the signal intensity of the uncapped fragment  $ppp\_AG\_p$  from s- and p-

RNA1, the uncapping rate can be measured as 10%, indicating that the capping efficiency was 90% (Figure 4D). In addition, when  $m^7G^{3'}mppp\_p(Am)G\_OH$ , which was generated by dephosphorylation after cleavage of p-RNA1 by RNase T1, was quantified by LC–MS using its commercially available product as a quantification standard, a similar value of 93.5% was obtained (Figure S3A), confirming that the method described above measures the 5' capping efficiency. Furthermore, analysis of mixtures of uncapped and capped RNAs at various ratios revealed that this method for measuring capping efficiency has quantitative linearity (Figure S3B).

**Poly(A) Tail Quantitation.** For quantitation of the poly(A) tail, the RNA of interest was cleaved with RNase T1, which does not result in cleavage of the poly(A) sequence. It thus remains as a long sequence among the nucleolytic fragments of the mRNA medicine product. We detected the long poly(A) RNA fragment by eluting it over a short period of time with a steep LC gradient (Figure S3C). In this case, the RNA was

engineered such that a guanosine is on the 3' side of the poly(A) sequence. The relative amount of 30 residue-poly(A) tail of p-RNA1 was determined as 1.00 by comparing that of s-RNA1. In addition, the poly(A) RNA fragment shorter than the entire length was not found among the p-RNA1 fragments (data not shown).

**Application of This Method to Mutated or Modified RNAs.** We then used this method to confirm the detection of defective RNAs. As RNAs for this purpose, we synthesized a version of p-RNA1 with a single-nucleotide substitution (p-RNA1mut), a version that was truncated (p-RNA1trn), and a version with an extra 12 nucleotides at the 3' end (p-RNA1ext) (Figure 2A, Table S2). These were mixed 1:1 with s-RNA1 and were analyzed by the above method. In the bubble charts obtained from these mutated or modified RNAs, most of the bubbles were detected as doublets, whereas several single bubbles were observed (Figure 5A). When the RNA sequences that resulted in these single bubbles were identified, they matched the sequences involved in the mutation (Figure S4A).

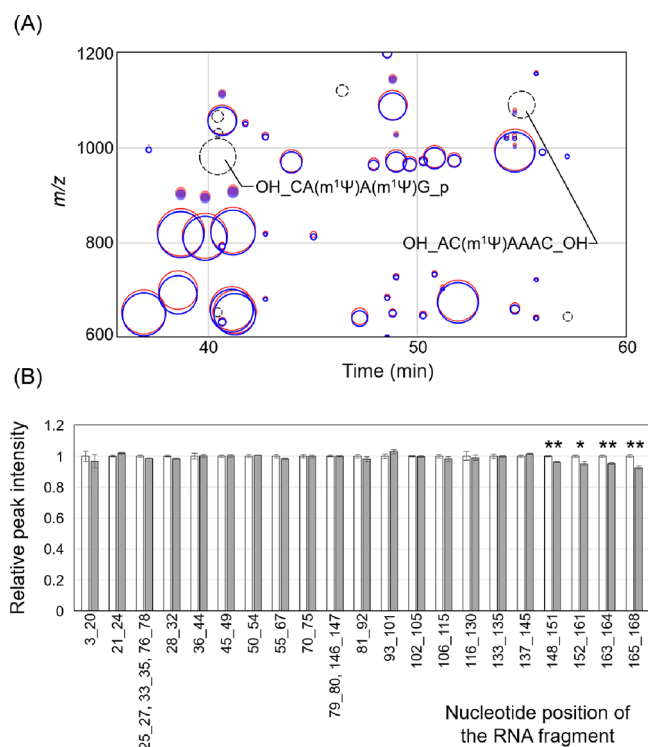


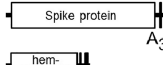
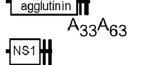
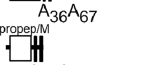
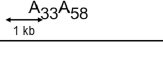
**Figure 5.** Detection of a defect in p-RNA1. (A) Bubble chart of the analysis of p-RNA1ext against s-RNA1. Only that region of the chart is shown that includes the singlet bubble derived from the extra sequence. Legend is the same as in Figure 3. Two bubbles labeled in the chart represent an extra sequence. (B) Measurement of contamination with a small amount of truncated p-RNA1. Purified p-RNA1 and the truncated form p-RNA1trn were mixed at a ratio of 100:0 or 95:5. This mixture (100 fmol) was further mixed with s-RNA1 at a ratio of 1:1. This 1:1 mixture was then digested with RNase T1, and the product was subjected to LC–MS and –MS/MS to identify RNA fragments and measure their mass chromatogram peak heights. The peak heights of each p-RNA1 and s-RNA1 fragment were normalized to the corresponding s-RNA1 fragment and were plotted with error bars (mean  $\pm$  standard error from three different experiments). The coefficient of variations of 100:0 (white bar) and 95:0 (shaded bar) mixtures were 1.92% and 1.69%, respectively. Significant differences were tested by the Student *t* test (\**p* < 0.05 and \*\**p* < 0.01).

In the case of the mixture that included RNA1ext, which contains the extra sequence OH\_CA(m<sup>1</sup>Ψ)A(m<sup>1</sup>Ψ)GAC-(m<sup>1</sup>Ψ)AAAC\_OH at the 3' end of RNA1, fragments corresponding to OH\_CA(m<sup>1</sup>Ψ)A(m<sup>1</sup>Ψ)G\_p and OH\_AC-(m<sup>1</sup>Ψ)AAAC\_OH were detected only from p-RNA1ext (Figure 5A). Thus, the platform should easily detect the mutated RNAs when substitutions in the template, truncation of the RNA product, or an extra sequence that results from read-through or loopback extension when double-strand RNA synthesis occurs.

During an actual synthesis situation, full-length products tend to be mixed with a small amount of shorter ones. To mimic this situation, we prepared samples of p-RNA1 mixed with a certain percentage of p-RNA1trn. When these samples were analyzed with s-RNA1 as a reference, a smaller amount of RNA fragments corresponding to the missing region was detected in proportion to the amount of RNA1trn added (Figure S4B). In particular, the method detected the missing portions of p-RNA1trn even when the p-RNA1 sample contained 5% of the truncated version (Figure 5B). These data indicate that our method is capable of detecting even small amounts of truncated products and revealing their missing sequences.

We also analyzed RNAs containing modified nucleosides such as Ψ or mo<sup>5</sup>U instead of uridine, and m<sup>5</sup>C instead of cytidine, referred to as RNA1mod1 and RNA1mod2, respectively (Figure 2). s- and p-RNA1mod1 and s- and p-RNA1mod2 were prepared by using the modified nucleoside triphosphate with the same template that encodes RNA1. Either s- and p-RNA1mod1 or s- and p-RNA1mod2 were mixed at a 1:1 ratio, which was then analyzed by the above method. The results confirmed that p-RNA1mod1 and p-RNA1mod2 have internal sequences that are identical to those of s-RNA1mod1 and s-RNA1mod2, respectively, and had similar capping and poly(A) efficiencies (Figure S5 and Table S4), indicating that the method was applicable regardless of the modified nucleoside type.

**Application to Long mRNA Reagents Including COVID-19 Vaccine-Like Molecules.** To assess the applicability of this analytical platform to long mRNA medicine-like molecules, we prepared RNAs ranging from 1.0 to 4.3 kb in length that encode surface antigens of SARS-CoV2 and influenza, Zika, and West Nile viruses (Figure 6). First, for the mRNA that encodes the COVID-19 antigens, we tested mimBNT162b2, which has the same sequence as BNT162b2 developed by Pfizer/BioNTech, for a COVID-19 vaccine except for a slightly different length of its poly(A) tail. The template DNA of mimBNT162b2 was constructed as described,<sup>6</sup> with the addition of the T7 promoter. s-mimBNT162b2 is 4.3 kb in length, lacks the capping structure, and contains m<sup>1</sup>Ψ and [<sup>13</sup>C<sub>10</sub>]G instead of uridine and G, respectively. After RPLC purification (Figure S6A), the RNA was characterized by LC–MS analysis, which indicated that there was a 100% sequence and quantitative coverage of the internal sequence (Figure S6B). The poly(A) tail was 65 to 70 nucleotides, with 68 nucleotides being the most common length (Figure S6C,D). In addition, we found a trace amount of fragments such as OH\_C(m<sup>1</sup>Ψ)(m<sup>1</sup>Ψ)(m<sup>1</sup>Ψ)(m<sup>1</sup>Ψ)(m<sup>1</sup>Ψ)\_OH and OH\_C(m<sup>1</sup>Ψ)(m<sup>1</sup>Ψ)(m<sup>1</sup>Ψ)(m<sup>1</sup>Ψ)(m<sup>1</sup>Ψ)(m<sup>1</sup>Ψ)\_OH. These were not included in the template sequence and thus appeared to be produced by loopback extensions involving the poly(A) sequence.

RNA	Structure	Coverage Ariadne/ manual (%)	Capping efficiency (%)	Poly(A) integrity (%)
mimBNT162b2		97/3 (49/4)	94	106
Influenza A		95/5 (70/7)	97	101
West Nile		90/10 (63/12)	96	98
Zika		89/11 (68/13)	80	92

**Figure 6.** Schematic structure of vaccine-like mRNAs used for assessment of the analytical platform. The white and black rectangles represent the protein-coding region and poly(A) region, respectively. The protein name and poly(A) length are written beside each square. Coverage shows the percentage of portions with both sequence and quantitative values, as identified manually with Ariadne. Coverage by unique oligonucleotides is shown in parentheses. The capping efficiency represents the percentage of mRNA 5' capped by the  $m^7G^{3'}ppp_{(Am)}G_{OH}$  reagent. Poly(A) integrity (%) of mimBNT162b and influenza A, Zika, and West Nile RNAs were calculated from the RNA fragments containing 67, 63, 67, and 58 poly(A) residues, respectively.

We then used the s-mimBNT162b2 RNA to analyze p-mimBNT162b2. Because we mixed equal amounts of s- and p-mimBNT162b2, the resulting bubble chart represented all

RNA fragments, except those corresponding to the 5' and 3' ends, at ratios of  $\sim 1:1$  (Figure 7). However, of the total 303 fragments generated by RNase T1 digestion of p-mimBNT162b2, 18 RNA fragments failed to be quantified due to signal overlap during LC-MS (Table S5). These were quantified by analysis using signals obtained by MS/MS and were found to contain approximately the same amount of  $^{13}C$ -labeled fragments as their counterparts produced from s-mimBNT162b2 (Table S5). The analysis also showed that the capping efficiency was 94% (Figure 6 and Figure S7). In addition, the poly(A) integrity measured at the  $A_{67}$  containing poly(A)-tail fragment was 100%. Both s- and p-mimBNT162b2 had a distribution of poly(A) lengths, although the amount of poly(A)-tail fragments for any specific length was about the same for s- and p-mimBNT162b2, indicating that the poly(A) integrity of both RNAs was essentially the same (Figure S6D). These results showed that this analytical platform is applicable for the analysis of vaccine-like long mRNAs.

Next, we prepared RNAs that encode surface antigens of influenza, Zika, and West Nile viruses (Figure 6 and Table S2). These p-RNAs were also transcribed with T7 RNA polymerase and have  $m^{15}P$ TP instead of UTP and include the cap 1 analog. The analyses of these mRNA-like molecules also showed identity to their s-RNAs and revealed their capping efficiency (Figure 6). These results indicated that the analytical platform is a useful tool for quantitative characterization of biochemi-

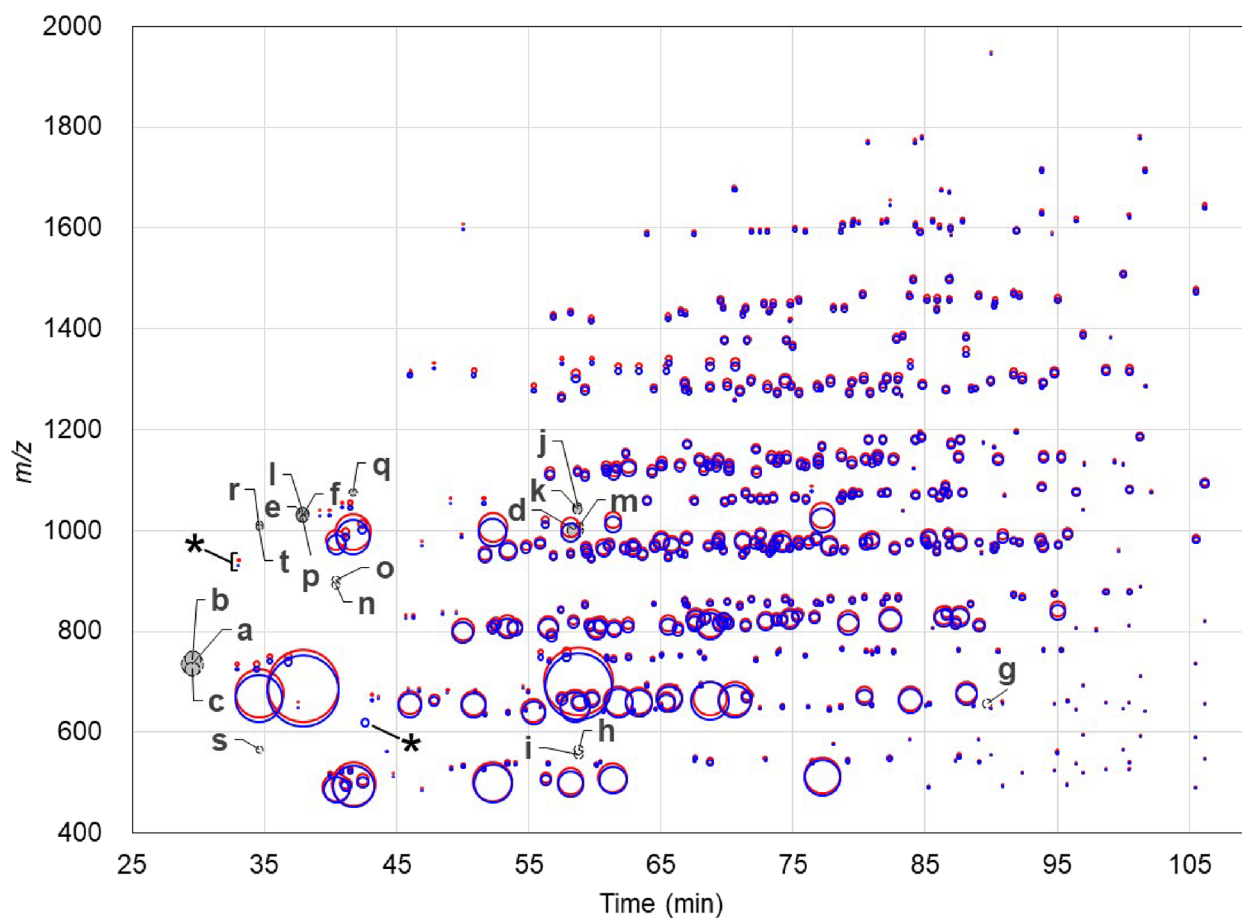


**Figure 7.** Bubble chart of the analysis of the p- and s-mimBNT162b2 RNAs. To simplify the chart, only those RNA ion bubbles without modifications that were not present in the synthesis, such as acOG, or adducts, are shown. Data are shown as in Figure 3. The assignment of each bubble (i.e., its short label) is presented in Table S5.

cally synthetic mRNA medicines in a size- and sequence-independent manner. Interestingly, with respect to the length of poly(A) tails, the influenza A RNA transcribed from the PCR-amplified template was more widely distributed than that transcribed from the plasmid template (Figure S8). Similar poly(A) distribution was observed in the Zika and West Nile RNAs (data not shown). This result indicated that transcription from a plasmid is more suitable for generating s-RNA than amplification by PCR for a poly(A) analysis.

## DISCUSSION

We have developed an analytical platform that has two steps for quality assessment of mRNA medicines. The first step involved establishing an isotope-labeled standard RNA through a detailed LC–MS/MS analysis. The second step compared an mRNA medicine to its standard based on LC–MS data of a 1:1 mixture. Once sufficient quantities of standard RNA are obtained during the first step, only two runs of the second step per sample, including the automated data analysis, provided all of the required information for the quality assessment, i.e., the efficiency of 5'-capping, the presence or absence of modified nucleotides in the internal sequence, and the length of the 3' poly(A) tail. This two-step setup thus allows for the rapid evaluation of mRNA medicines.

This method is highly applicable and is used for a wide variety of multiple nucleosides, sequences of different origins, and sequence lengths ranging from 0.2 to 4.3 kb (Figure 6). However, as RNase T1 is used in the second step, quantification of contiguous G sequences is not feasible. Such sequences can be quantified by labeling the U and C residues of the s-RNA with appropriate stable isotopes and using RNase A, which cleaves on the 3' side of pyrimidines, instead of labeling G residues and digesting RNA with RNase T1. Such a variant of SILNAS has already been used in rRNA sequencing<sup>33</sup> and should also be feasible for carrying out quality checks of mRNA medicines.

There are two methods for in vitro capping of RNA: co-transcriptional capping and post-transcriptional capping. Co-transcriptional capping is carried out by a one-step reaction in which a cap reagent is added during in vitro transcription and is introduced into the RNA by T7 polymerase, as described here. In contrast, post-transcriptional capping requires a multi-step reaction: RNA triphosphatase removes a monophosphate from the triphosphate group at the 5' end of a nascent RNA, at which point the capping enzyme subsequently links guanosine monophosphate, and then guanine N7-methyltransferase methylates the capping guanine.<sup>34</sup> Our quantitative method using SILNAS is not suitable as a method to quantify the capping efficiency of the post-transcriptional capping method. This is because post-transcriptional capping produces multiple intermediate products, and thus quantification of the triphosphorylated RNA does not reveal the capping efficiency. In such a case, the method demonstrated in Figure S3A is suitable for quantification. In this method, the purified mRNA medicine was digested with RNase T1/phosphatase, RNase A/phosphatase, or nuclease P1, and the resulting cap fragment was measured by LC–MS using the cap analog as the standard. In addition to m<sup>7</sup>G<sup>3'</sup>m(Am)G\_OH, the cap analogs m<sup>7</sup>Gppp\_A\_OH, m<sup>7</sup>Gppp\_G\_OH, m<sup>7</sup>G<sup>3'</sup>mppp\_G\_OH, OH\_m<sup>7</sup>Gppp\_(Am)U\_OH, and OH\_m<sup>7</sup>Gppp\_(Am)G\_OH are commercially available,<sup>2</sup> allowing various caps to be readily measured.

Two other methods have been reported for quantifying post-transcriptional capping. One is a method in which the RNA of interest is annealed with a complementary biotinylated tag at its 5' end; the resulting biotinylated RNA is cleaved with the DNA 3' end-directing activity of RNase H, and the hybrid fragments are purified for analysis by LC–MS.<sup>35</sup> Although this method can detect 0.5–25% uncapped RNA among an aliquot of an RNA, large amounts (100 pmol) of the capped RNA sample are required. The other method involves incorporating [ $\alpha$ -<sup>32</sup>P]GTP during in vitro transcription,<sup>36</sup> which results in a radioactive product that is therefore not suitable for clinical applications.

For measuring poly(A) tail lengths, two major methods are used in addition to cDNA sequencing. One method relies on northern blots and uses gene-specific oligonucleotides to induce RNase H cleavage more than 100 bases upstream of the polyadenylation site of the mRNA of interest.<sup>37</sup> The cleavage releases a short fragment of RNA, which is then analyzed by high-resolution visualization on an acrylamide northern blot. The other approach involves the addition of a defined sequence to the 3' end of the RNA and subsequent amplification by PCR. A linker is enzymatically added to the 3' end of the RNA that contains either G or inosine residues.<sup>37,38</sup> The length of the poly(A) tail is determined by amplifying the sequence between the added 3' linker and the intrinsic sequence upstream of the polyadenylation site. All of these methods involve multiple steps and are indirect measures that rely on hybridization to detect RNA or amplification of complementary DNA by PCR. The method presented here is a direct analysis of RNA and requires fewer steps, making it more suitable for the analysis of mRNA medicines than those earlier methods.

The method provided in this study is only a method to show the identity of the standard s-RNA and the pharmaceutical p-RNA. Short s-RNAs are able to purify sufficiently, and p-RNA can also be confirmed to have sufficient purity and integrity using such s-RNA. In contrast, when analyzing longer RNAs, the s-RNA purification may not be sufficient and the extra RNAs are difficult to identify. While this is a limitation of this method, it enables to show identity to the standard. Therefore, this method is effective for checking the identity of mRNA medicines produced at different times, i.e., for lot check.

mRNA medicines must possess a sufficient level of integrity, as underscored by the documents leaked from the European Medicines Agency that expressed concerns over unexpectedly low quantities (>55%) of intact mRNA in batches of the vaccine developed for commercial production.<sup>39</sup> These products may contain truncated forms derived from degradation or elongation defects or may be contaminated with additional sequences derived from double-stranded RNA generated by loopback extensions that is a byproduct of in vitro transcription and can stimulate expression of inflammatory cytokines.<sup>40,41</sup> These deficiencies have not been elucidated previously because of the absence of appropriate measurement methods. In this context, we believe the platform described here will immediately facilitate quality control of mRNA medicines, including batch-to-batch comparisons critical for long-term quality control, in addition to the method proposed by D'Ascenzo et al.<sup>17</sup>



## ■ ASSOCIATED CONTENT

### SI Supporting Information

The Supporting Information is available free of charge at <https://pubs.acs.org/doi/10.1021/acs.analchem.2c04323>.

(Table S1) Sequences; (Table S2) overlap extension PCR was performed to produce an in vitro transcription template; (Table S3) assignment of each bubble; (Table S4) p-RNA1mod1 and p-RNA1mod2, which have internal sequences that are identical to those of s-RNA1mod1 and s-RNA1mod2, respectively, and had similar capping and poly(A) efficiencies; (Table S5) 18 RNA fragments failed to be quantified due to signal overlap during LC–MS (XLSX)

(Figure S1) Purification and characterization of s-RNA1; (Figure S2) representative cases of pairs of mass signals obtained from the SILNAS analysis of p- and s-RNA1; (Figure S3) cap and poly(A) analysis of p-RNA1; (Figure S4) analysis of mutated or modified p-RNA1s using the platform described here; (Figure S5) analysis of RNAs containing modified nucleosides Ψ or mo5U instead of uridine and m5C instead of cytidine; (Figure S6) purification and characterization of s-mimBNT162b2; (Figure S7) cap and poly(A) analysis of p-mimBNT162b2; (Figure S8) poly(A) distribution among purified s- and p-influenza A RNA fragments (PDF)

## ■ AUTHOR INFORMATION

### Corresponding Author

Masato Taoka – Department of Chemistry, Graduate School of Science, Tokyo Metropolitan University, Hachioji-shi, Tokyo 192-0397, Japan; [orcid.org/0000-0001-5554-4951](https://orcid.org/0000-0001-5554-4951); Email: [mango@tmu.ac.jp](mailto:mango@tmu.ac.jp)

### Authors

Hiroshi Nakayama – Biomolecular Characterization Unit, RIKEN Center for Sustainable Resource Science, Wako-shi, Saitama 351-0198, Japan

Yuko Nobe – Department of Chemistry, Graduate School of Science, Tokyo Metropolitan University, Hachioji-shi, Tokyo 192-0397, Japan

Masami Koike – Biomolecular Characterization Unit, RIKEN Center for Sustainable Resource Science, Wako-shi, Saitama 351-0198, Japan

Complete contact information is available at:

<https://pubs.acs.org/doi/10.1021/acs.analchem.2c04323>

### Author Contributions

<sup>#</sup>H.N. and Y.N. contributed equally. The manuscript was written through contributions of all authors. All authors have given approval to the final version of the manuscript.

### Notes

The authors declare no competing financial interest.

## ■ REFERENCES

- (1) Beck, J. D.; Reidenbach, D.; Salomon, N.; Sahin, U.; Türeci, Ö.; Vormehr, M.; Kranz, L. M. *Mol. Cancer* **2021**, *20*, 69.
- (2) Qin, S.; Tang, X.; Chen, Y.; Chen, K.; Fan, N.; Xiao, W.; Zheng, Q.; Li, G.; Teng, Y.; Wu, M.; et al. *Signal Transduction Targeted Ther.* **2022**, *7*, 166.
- (3) Barbier, A. J.; Jiang, A. Y.; Zhang, P.; Wooster, R.; Anderson, D. G. *Nat. Biotechnol.* **2022**, *40*, 840–854.

- (4) Berraondo, P.; Martini, P. G. V.; Avila, M. A.; Fontanellas, A. *Aut* **2019**, *68*, 1323–1330.
- (5) Pardi, N.; Hogan, M. J.; Porter, F. W.; Weissman, D. *Nat. Rev. Drug Discovery* **2018**, *17*, 261–279.
- (6) Nance, K. D.; Meier, J. L. *ACS Cent. Sci.* **2021**, *7*, 748–756.
- (7) Fang, E.; Liu, X.; Li, M.; Zhang, Z.; Song, L.; Zhu, B.; Wu, X.; Liu, J.; Zhao, D.; Li, Y. *Signal Transduction Targeted Ther.* **2022**, *7*, 94.
- (8) Iavarone, C.; O'hagan, D. T.; Yu, D.; Delahaye, N. F.; Ulmer, J. B. *Expert Rev. Vaccines* **2017**, *16*, 871–881.
- (9) Schlake, T.; Thess, A.; Fotin-Mlecsek, M.; Kallen, K. J. *RNA Biol.* **2012**, *9*, 1319–1330.
- (10) To, K. K. W.; Cho, W. C. S. *Expert Opin. Drug Discovery* **2021**, *16*, 1307–1317.
- (11) Karikó, K.; Buckstein, M.; Ni, H.; Weissman, D. *Immunity* **2005**, *23*, 165–175.
- (12) Tanji, H.; Ohto, U.; Shibata, T.; Taoka, M.; Yamauchi, Y.; Isobe, T.; Miyake, K.; Shimizu, T. *Nat. Struct. Mol. Biol.* **2015**, *22*, 109–115.
- (13) Yan, K.; Zhu, W.; Yu, L.; Li, N.; Zhang, X.; Liu, P.; Chen, Q.; Chen, Y.; Han, D. *Mol. Cell. Endocrinol.* **2013**, *372*, 73–85.
- (14) Gallie, D. R. *Genes Dev.* **1991**, *5*, 2108–2116.
- (15) Jiang, T.; Yu, N.; Kim, J.; Murgo, J.-R.; Kissai, M.; Ravichandran, K.; Miracco, E. J.; Presnyak, V.; Hua, S. *Anal. Chem.* **2019**, *91*, 8500–8506.
- (16) Vanhinsbergh, C. J.; Criscuolo, A.; Sutton, J. N.; Murphy, K.; Williamson, A. J. K.; Cook, K.; Dickman, M. J. *Anal. Chem.* **2022**, *94*, 7339–7349.
- (17) D'Ascenzo, L.; Popova, A. M.; Abernathy, S.; Sheng, K.; Limbach, P. A.; Williamson, J. R. *Nat. Commun.* **2022**, *13*, 2424.
- (18) Wolf, E. J.; Grünberg, S.; Dai, N.; Chen, T.-H.; Roy, B.; Yigit, E.; Corrêa, I. R. *Nucleic Acids Res.* **2022**, *50*, e106–e106.
- (19) Taoka, M.; Nobe, Y.; Hori, M.; Takeuchi, A.; Masaki, S.; Yamauchi, Y.; Nakayama, H.; Takahashi, N.; Isobe, T. *Nucleic Acids Res.* **2015**, *43*, e115–e115.
- (20) Nakayama, H.; Akiyama, M.; Taoka, M.; Yamauchi, Y.; Nobe, Y.; Ishikawa, H.; Takahashi, N.; Isobe, T. *Nucleic Acids Res.* **2009**, *37*, e47–e47.
- (21) Nakayama, H.; Takahashi, N.; Isobe, T. *Mass Spectrom. Rev.* **2011**, *30*, 1000–1012.
- (22) Trepotec, Z.; Geiger, J.; Plank, C.; Aneja, M. K.; Rudolph, C. *RNA* **2019**, *25*, 507–518.
- (23) Grier, A. E.; Burleigh, S.; Sahni, J.; Clough, C. A.; Cardot, V.; Choe, D. C.; Krutein, M. C.; Rawlings, D. J.; Jensen, M. C.; Scharenberg, A. M.; et al. *Mol. Ther.–Nucleic Acids* **2016**, *5*, No. e306.
- (24) Tautz, D.; Schlötterer, C. *Curr. Opin. Genet. Dev.* **1994**, *4*, 832–837.
- (25) Hilgarth, R. S.; Lanigan, T. M. *MethodsX* **2020**, *7*, 100759.
- (26) Fazekas, A.; Steeves, R.; Newmaster, S. *BioTechniques* **2010**, *48*, 277–285.
- (27) Shinde, D.; Lai, Y.; Sun, F.; Arnheim, N. *Nucleic Acids Res.* **2003**, *31*, 974–980.
- (28) Yamauchi, Y.; Taoka, M.; Nobe, Y.; Izumikawa, K.; Takahashi, N.; Nakayama, H.; Isobe, T. *J. Chromatogr. A* **2013**, *1312*, 87–92.
- (29) Taoka, M.; Yamauchi, Y.; Nobe, Y.; Masaki, S.; Nakayama, H.; Ishikawa, H.; Takahashi, N.; Isobe, T. *Nucleic Acids Res.* **2009**, *37*, e140–e140.
- (30) Nakayama, H.; Yamauchi, Y.; Taoka, M.; Isobe, T. *Anal. Chem.* **2015**, *87*, 2884–2891.
- (31) Boccaletto, P.; Machnicka, M. A.; Purta, E.; Piatkowski, P.; Baginski, B.; Wirecki, T. K.; de Crecy-Lagard, V.; Ross, R.; Limbach, P. A.; Kotter, A.; et al. *Nucleic Acids Res.* **2018**, *46*, D303–D307.
- (32) Thomas, B.; Akoulitchev, A. V. *Trends Biochem. Sci.* **2006**, *31*, 173–181.
- (33) Taoka, M.; Nobe, Y.; Yamaki, Y.; Sato, K.; Ishikawa, H.; Izumikawa, K.; Yamauchi, Y.; Hirota, K.; Nakayama, H.; Takahashi, N.; et al. *Nucleic Acids Res.* **2018**, *46*, 9289–9298.
- (34) Muttach, F.; Muthmann, N.; Rentmeister, A. *Beilstein J. Org. Chem.* **2017**, *13*, 2819–2832.

- (35) Beverly, M.; Dell, A.; Parmar, P.; Houghton, L. *Anal. Bioanal. Chem.* **2016**, *408*, 5021–5030.
- (36) Grudzien, E.; Stepinski, J.; Jankowska-Anyszka, M.; Stolarski, R.; Darzynkiewicz, E.; Rhoads, R. E. *RNA* **2004**, *10*, 1479–1487.
- (37) Nilsen, T. W. *Cold Spring Harb. Protoc.* **2015**, *2015*, 413–418.
- (38) Kusov, Y. Y.; Shatirishvili, G.; Dzagurov, G.; Gauss-Müller, V. *Nucleic Acids Res.* **2001**, *29*, E57–E57.
- (39) Tinari, S. *BMJ* **2021**, *372*, n627.
- (40) Gholamalipour, Y.; Karunanayake Mudiyansele, A.; Martin, C. T. *Nucleic Acids Res.* **2018**, *46*, 9253–9263.
- (41) Karikó, K.; Muramatsu, H.; Ludwig, J.; Weissman, D. *Nucleic Acids Res.* **2011**, *39*, No. e142.